USE OF SYNCHRONIZED, INFRARED THERMOMETRY AND HIGH-SPEED VIDEO FOR GENERATION OF SPACE- AND TIME- RESOLVED HIGH-QUALITY DATA ON BOILING HEAT TRANSFER

Craig Gerardi, Hyungdae Kim, Jacopo Buongiorno*

Massachusetts Institute of Technology
77 Massachusetts Ave., 24-206
Cambridge MA 02141, * 1(617)253-7316 jacopo@mit.edu

Abstract
Boiling heat transfer is a key thermal limit in nuclear systems. However, for decades, its modeling has relied on speculative hypotheses and a good dose of empiricism. As researchers now start to develop more mechanistic models, the need for high-quality high-resolution data on the bubble nucleation and growth cycle is increasing. Specifically, nucleation site density, bubble departure diameter and frequency data, are necessary input for and validation of the source terms in interfacial area transport models, CFD 'multi-fluid' models, as well as direct numerical simulation models of boiling based on interface tracking methods. In this paper we present an approach based on *synchronized* infrared thermometry and high-speed video 'through' the heater that enables simultaneous measurement of the nucleation site density, bubble growth rate (including bubble departure diameter), bubble departure frequency (including wait time), time-resolved 2D temperature distribution and phase distribution on the boiling surface, all in a relatively effortless manner.

1. INTRODUCTION

The economic potential of the Light Water Reactor (LWR) technology has been hindered by a lack of fundamental understanding of key multiphase flow and heat transfer phenomena, such as subcooled flow boiling, departure from nucleate boiling, dryout, quenching, multi-dimensional natural circulation, etc. For lack of a better approach, the reactor designers and safety analysts have adopted "supersized" margins to the postulated limits, which have resulted in the deployment of LWR plants that perform below their intrinsic potential. Current design and safety codes almost exclusively use multiphase flow and heat transfer models/correlations that are still highly empirical: in particular, they rely on empirical heat transfer coefficient correlations to calculate the vapor generation rate, and then simple semi-empirical models for bubble drag, condensation, breakup and coalescence are used, all assuming idealized geometries of the vapor/liquid interface, i.e. spherical or elliptical or otherwise symmetric bubbles (Ishii and Hibiki, 2006). The physical reality of the situation is of course much more complex, as shown by any direct visualization of the phenomena. The geometry of the liquid/vapor interface is highly irregular and its nature is dynamic; also, rapid changes in interface geometry generate turbulence, which cannot be captured by the traditional single-phase turbulence models.

Revolutionary advancements in modeling and simulation of multiphase flow and heat transfer phenomena are available through the use of Interface Tracking Methods (ITM) (Prosperetti and Tryggvason, 2007). In ITMs, the traditional single-phase problem of solving the Navier-Stokes equations, to find the velocity and pressure fields, is coupled to the problem of finding how a marker function, which defines the vapor/liquid interface, evolves vs time and position. Different ITMs differ in the way the marker function is advected and the interface reconstructed. Popular ITMs include the Volume of Fluid (VOF) method (Scardovelli and Zaleski, 1999; Rudman, 1998; Rider and Kothe, 1998), the level-set method (Psher and Fedkiw, 2001; Sethian, 2001) and the front tracking method (Tryggvason et al., 2001; Du et al., 2006). ITMs avoid unphysical sharp transitions between flow regimes, and, importantly, do not assume idealized geometries for the interfaces between phases. Moreover, ITMs can resolve the velocity and temperature

gradients near the interface (through Direct Numerical Simulation, DNS, or Large Eddy Simulation, LES), so prediction of the exchange of momentum and heat at the interface requires no empirical correlations. The physical complexity of the two-phase flow and heat transfer phenomena encountered in LWR systems naturally lends itself to an ITM analysis approach. Examples of ITM-based simulations of two-phase flow and heat transfer phenomena are shown in Fig. 1.

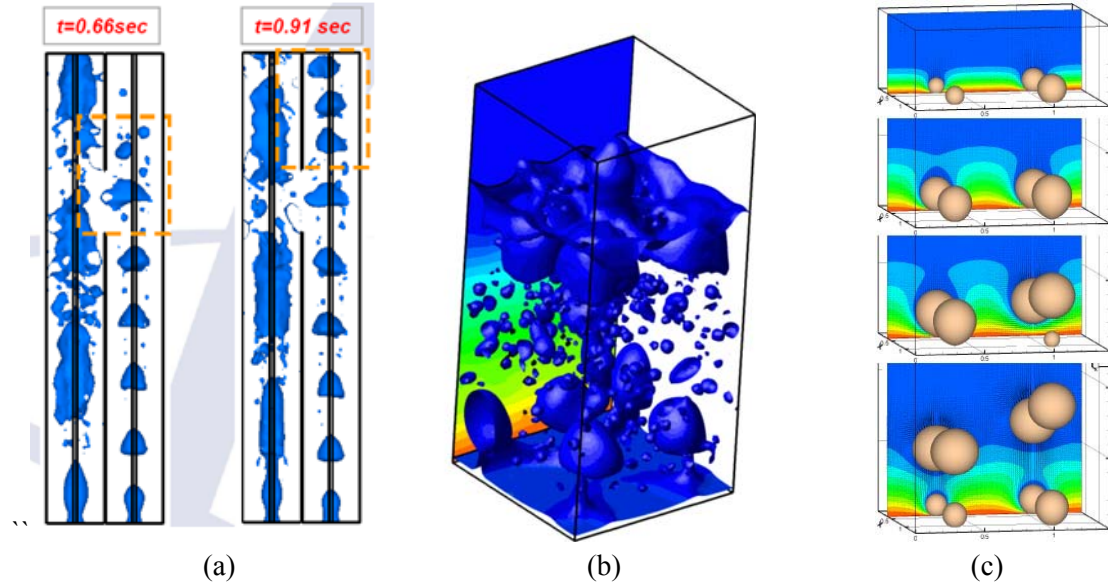<center>(a)   (b)   (c)</center>

Fig 1. (a) VOF simulation of plug flow in parallel channels (courtesy of Dr Emilio Baglietto, CD-Adapco), (b) level-set simulation of film boiling from a flat surface (courtesy of Dr Djamel Lakehal, Ascomp GmbH), (c) Front-tracking simulation of bubbles simultaneously growing at and detaching from four prescribed nucleation sites (courtesy of Prof Gretar Tryggvason, WPI).

At MIT we are undertaking a research program whose objectives are to develop and validate ITM-based models of multiphase flow and heat transfer, and apply them to LWR design and safety. Recognizing that it is not possible to tackle all phenomena and effects at the same time, the program has started from one of the most important phenomena in LWRs, i.e. nucleate boiling heat transfer.

In this context, we hereby present an experimental technique that can be used to generate data, highly-resolved in space and time, needed to validate ITM-based (as well as more traditional) models of boiling heat transfer. The technique is described in Section 2. Examples of the data obtainable with such technique are presented in Section 3. The value of the data is discussed in Sections 4 and 5.

2. DESCRIPTION OF SYNCHRONIZED HIGH-SPEED INFRARED-THERMOMETRY AND VIDEO TECHNIQUE

2.1 Facility Description
Boiling experiments are conducted in the facility shown in Fig. 2. A thin film made of Indium-Tin-Oxide (ITO) is electrically heated. Boiling occurs on the upward facing side of this film which has an exposed area of 30x10 mm^2, is 0.7 μm thick and has a surface roughness SRa=30 nm. The ITO is vacuum deposited onto a 0.4 mm thick sapphire substrate. This heater is connected to a DC power supply to control the heat flux at the surface. The cell accommodating the test fluid is sealed, included a condenser, and is surrounded by a constant-temperature water bath to maintain a constant test-fluid temperature by minimizing heat losses to the ambient. Acquisition of the temperature distribution on the heater surface is accomplished using an infrared (IR) high-speed camera, SC 6000 from FLIR Systems, Inc. The use of an

IR camera to investigate boiling heat transfer was pioneered by Theofanous et al. (2002). However, in our system simultaneous high-speed video (HSV) is taken with a high-speed digital imaging system, Phantom v7.1 from Vision Research. A function generator produces a transistor-transistor logic (TTL) pulse at 500 Hz which triggers both cameras to simultaneously record an image allowing the synchronization of both cameras' image sequences. A custom hybrid hot mirror (dichroic) is placed directly below the heater which reflects the IR (3-5 μm) spectrum to the IR camera and transmits the visible (400-700 nm) spectrum. The visible spectrum that passes through the hybrid hot mirror is then reflected by a silver-coated mirror to the HSV system. Thus, both cameras image the area of interest from the same point of view. While the sapphire substrate is transparent (>85%) to IR light, the ITO has the advantageous property of being opaque in the IR range, as this ensures that all temperature measurements are made on the back (bottom) of the ITO substrate. The thinness of the ITO heater guarantees that the IR camera reading from its bottom is an accurate representation of the actual temperature on the top (wet side) of the heater surface. Thus, neither the temperature of the fluid, nor the integral temperature through the substrate thickness is measured. This makes thermal analysis of the heater, and corresponding temperature measurements straightforward. Heat loss from the heater bottom via air natural convection was calculated to be negligible (<1%).

As configured in this study, the IR camera and HSV system have spatial resolutions of 100 μm and 50 μm respectively. In the case of the IR image, this resolution is more than sufficient to capture the temperature history of individual bubble nucleation events at the nucleation sites since the typical bubble diameter is on the order of 1000 μm. The frame rate of both cameras is 500 Hz. During each experiment, the heat flux is increased in discrete steps up to the critical heat flux (CHF). At each intermediate step the temperature map and visualization are concurrently recorded for 1.0 sec. Since the typical time scale for a bubble nucleation cycle is tens of ms, 1 sec is sufficient to obtain good data statistics.
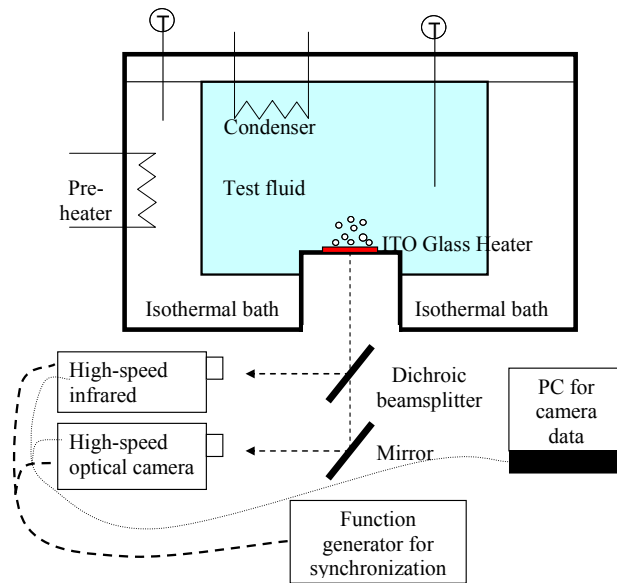

Fig 2: MIT pool boiling facility with infrared thermometry and high-speed video cameras.

3. DATA

3.1 Data Reduction and Uncertainty
The raw data obtained for each heat flux are in the form of hundreds of frames, each representing a two-dimensional infrared intensity distribution on the heater surface (see Fig. 3). The conversion from IR intensity to temperature is done via a calibration curve, obtained using vendor-supplied blackbody

simulators; with an accuracy of about 2%, or 2°C. The nucleation sites appear as short-lived dark (cold) spots on the IR image. The edge of the nucleation sites is sharp because there is very little radial conduction within the heater, as discussed above. The nucleation sites in each frame are marked manually, to ensure no nucleation site is missed; then the nucleation site density can be determined simply as the total number of nucleation sites divided by the area of the heater. The bubble departure diameter is measured from the maximum size of the cold spot. Note that here the bubble diameter is actually the thermal foot-print of the bubble, i.e., the bottom of the bubble that is in contact with the heater surface. The actual bubble departure size is typically larger and can be measured with the HSV. If only the infrared data along a chord cutting through a nucleation site are considered, the one-dimensional temperature distribution vs. time of Fig. 4 is obtained. Further, if the spatial average of the temperature at a given nucleation site is calculated and plotted vs. time, then various features of the bubble cycle, such as the bubble departure frequency, bubble growth time and bubble wait time become apparent and can be readily estimated (see Fig. 5). Since boiling is essentially a random phenomenon, for each nucleation site, there is a distribution of the parameters; however, we observed that the parameters tend to be distributed normally and narrowly about their mean.   Typical uncertainties are estimated to be about 2% for nucleation site density, 10% for the bubble departure diameter, 20% for the bubble frequency, and 20% for the bubble growth and wait times. In the remainder of the paper we will use only the mean values for all these parameters, but the associated uncertainties should be kept in mind. More details on the data reduction and uncertainties can be found in Gerardi (2009).
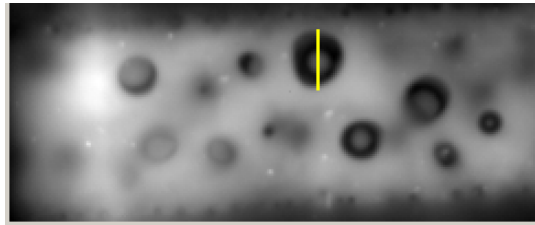

Fig. 3: Sample screenshot of selecting the diameter of a nucleation site (yellow line bisects diameter). Nucleation sites appear as dark (cold) spots in IR images.
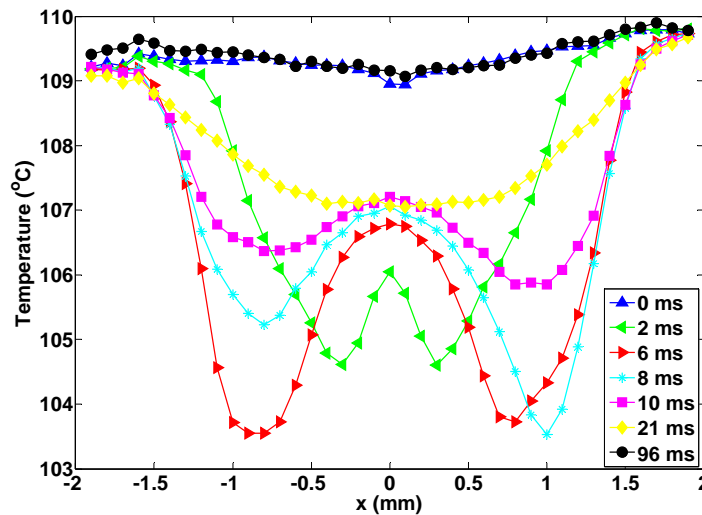

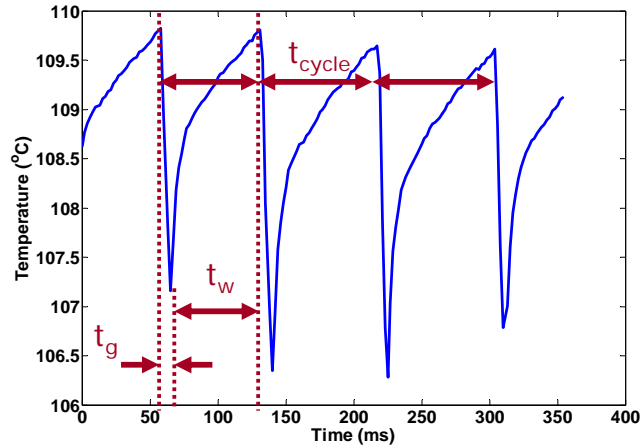Fig. 4. 1D temperature distribution on the heater surface underneath a growing bubble.

Fig. 5: Temperature response below individual nucleation site showing frequency response of nucleation cycle. Average temperature of entire nucleation site is used. Note the characteristic slow heating and sudden cooling cycles, which are expected during a bubble nucleation event. t_{cycle} is the sum of the growth time, t_g, and wait time, t_w. The average value of the cycle times can be used to find the characteristic bubble departure frequency ($f_b=1/t_{cycle}$).

3.2 Bubble Nucleation and Growth Data

A single representative bubble cycle is chosen from the synchronized experiments and the HSV and IR for this bubble are shown in Fig. 6. The HSV shown in Fig. 6(a) visually depicts bubble growth. The depth of field for this particular camera setup is sufficient to see several millimeters past the heater surface, thus capturing the shape and size of the bubble even as it detaches from the heater surface. To interpret these data, it is useful to refer to the commonly accepted model for bubble growth at a boiling surface, which is shown in Fig 7. The actual outer radius of the bubble, R_t, and the microlayer (hemispherical) radius, r_c, are clearly visible in the images of Fig. 6(a). Both the microlayer radius and dry spot radius are measured using the IR images as shown in Fig. 6(b). The microlayer radius is taken to be the cooled (thus dark colored) circular expanding area. The dry out area is taken to be the hotter (thus light colored) circular area that expands as the microlayer evaporates in the center of the cooled circular area. Initial hemispherical growth is confirmed by the HSV of Fig. 6(a). Specifically, frame 48 shows that the outer bubble radius, R_t, and the hemispherical microlayer radius, r_c, have approximately the same value, suggesting that the initial bubble growth is primarily in the radial direction along the surface. Contrast this with later frames (49-51), where the outer bubble radius is significantly larger than the hemispherical radius. Zhao et al. (2002) developed an expression for the radius of the dryout area as a function of bubble growth time which expanded upon the theoretical and experimental analysis of microlayer growth by Cooper and Lloyd (1969). The Cooper and Loyd (1969) expression for the hemispherical bubble radius and the Zhao et al. (2002) expression for microlayer dryout radius are compared with the cold spot and hot spot radii as measured using the infrared camera for q"=60kW/m^2 in Fig. 8. Data for five bubbles from the same experiment were considered in order to show a clearer picture of bubble growth variability. The average radii values are represented by the data point, while the error bars represent the minimum and maximum radii of the five bubbles considered. Measurement error is ±10%. The existence of a centrally expanding hot spot in the IR images, and the bubble growth analysis confirms the existence of microlayer evaporation during nucleate boiling in water through the direct measurement of surface temperature during bubble growth. A previous study by Koffman and Plesset (1983) used laser interferometry to record microlayer evaporation, but had a large amount of uncertainty due to the measurement technique (e.g. interpretation of fringe patterns). The technique based on

5

synchronized IR thermography and HSV is shown here to be an effective method of directly measuring the movement of the three-phase contact line during microlayer evaporation.
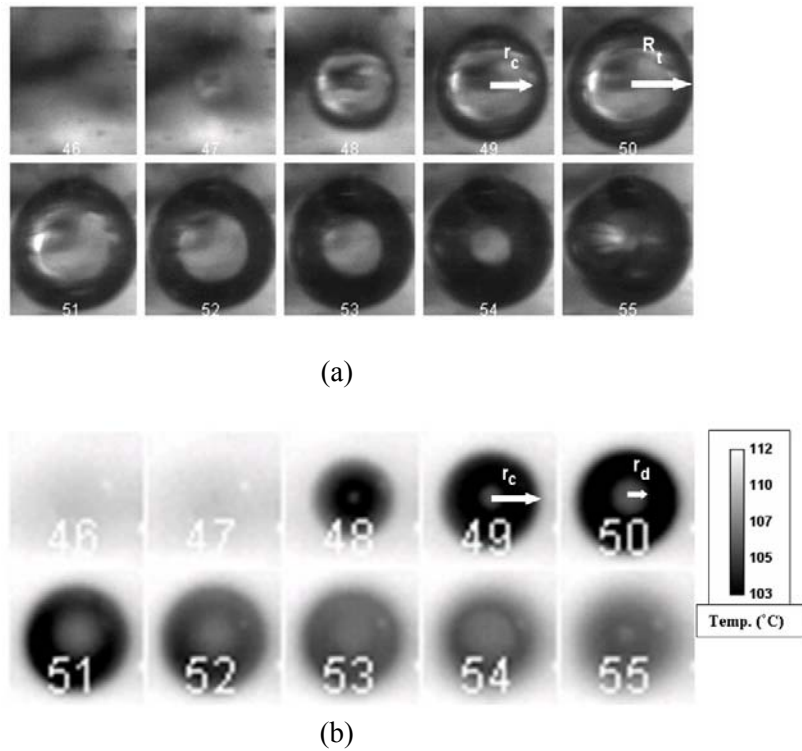

(a)

(b)

Fig. 6: (a) High speed video (HSV) and (b) infrared (IR) temperature data for a single bubble life-cycle. Frames 46-55 are shown for deionized water at q"=60kW/m^2, with the time interval between consecutive images being ~2.08ms. Bubble incipience is seen in frame 47 on the HSV, end of bubble growth in frame 51 and complete bubble departure at frame 55. The IR data show the bubble thermal footprint growing in frames 48-51, and a central expanding "hot" region corresponding to the evaporation of the microlayer and growth of the dryout region.
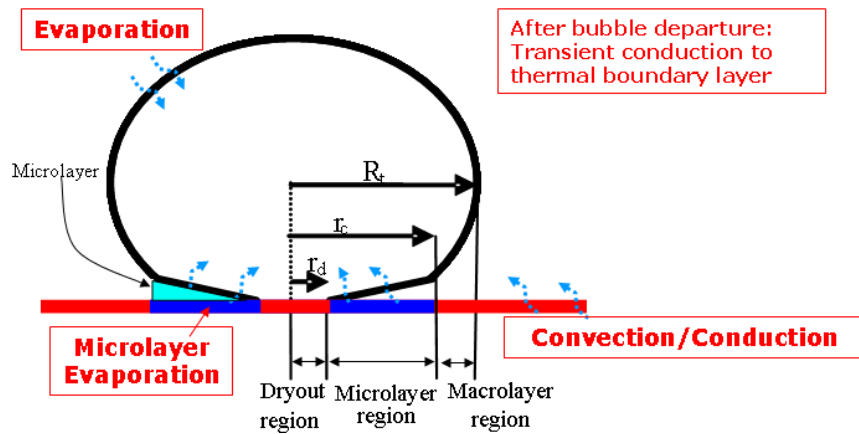

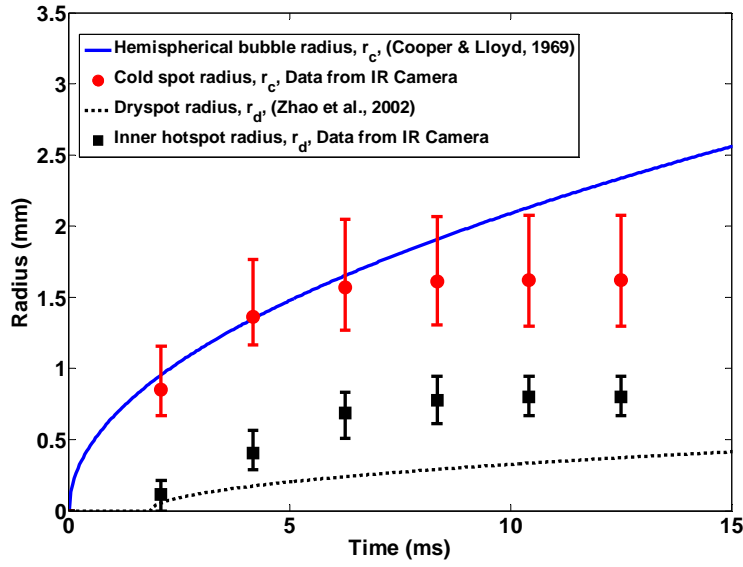Fig. 7: Schematic of a growing bubble and related heat transfer mechanisms.

Fig. 8: Comparison of cold spot and hot spot radii growth for 5 bubbles with corresponding predictions for DI water at q"=60kW/m^2. Error bars represent minimum and maximum measured values in order to show experimental spread. Measurement error ±10%

3.3 Phase Distribution on the Boiling Surface

An interesting variant of the technique described above is one in which the ITO-sapphire heater is replaced with a silicon wafer (optical grade, P/Boron-doped, thickness 380±25 μm, double side polished), which is transparent (~55%) to IR light, while water has a very high IR absorbivity (e.g. water). Therefore, where the heater surface is wet, the IR camera measures the temperature of the hot water in contact with the heater. On the other hand, where vapor (whose IR absorbivity is very low) is in contact with the heater, the IR light comes from the cooler water beyond the vapor. The resulting IR image appears dark (cold) in dry spots and bright (hot) in wetted area. Using the contrast between the dark and bright areas, we can visualize the distribution of the liquid and gas phases in contact with the heater surface. In other words, we measure temperature *beyond* the surface to detect phases *on* the surface. A particularly simple application is shown in Fig. 9.
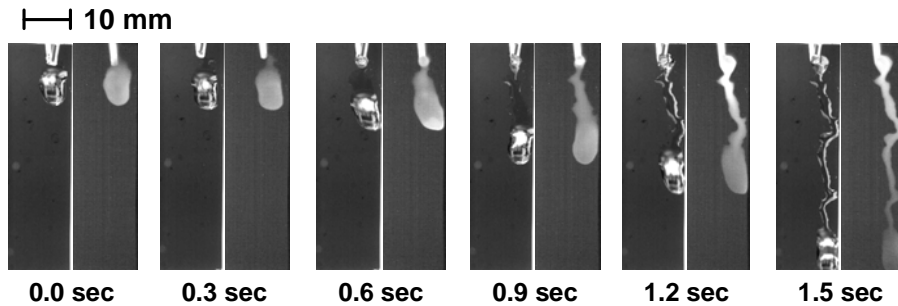

Fig. 9: Droplet sliding on a vertical silicon wafer. Comparison of the HSV (left) and IR (right) images taken from the front and back of the wafer, respectively. The liquid was pre-heated to ~30°C, while the wafer and background were at room temperature (~24°C); as a result, in the IR video the sliding droplet appears brighter than the background, and thus easily distinguishable. The sharpness of the IR image through the wafer confirms that the wafer is transparent to IR.

A more complex physical situation is shown in Fig. 10, where the highly irregular and dynamic phase distribution on the boiling surface is captured as a function of time for q"~500 kW/m². Note that large areas of the heater surface appear dry and stay dry for long periods of time (order of 30 ms), though at this heat flux we are still well below CHF, which occurred at ~1100 kW/m² on our silicon wafer heater. An important caveat: because the penetration length of IR light in the 3-5 μm range can be up to 100 μm, we cannot categorically exclude that a very thin liquid film (<<100 μm thick) exists in the 'dry' patches. However, in their boiling experiments with ethanol and refrigerants, Nishio and Tanaka (2004) and Chung and No (2003), who used the total reflection approach, also observed large dry areas similar to ours. The wetted area fraction (defined as the ratio of the liquid area to the total surface area) can be obtained by processing of the IR images, and is shown for different values of the heat flux in Fig. 11.
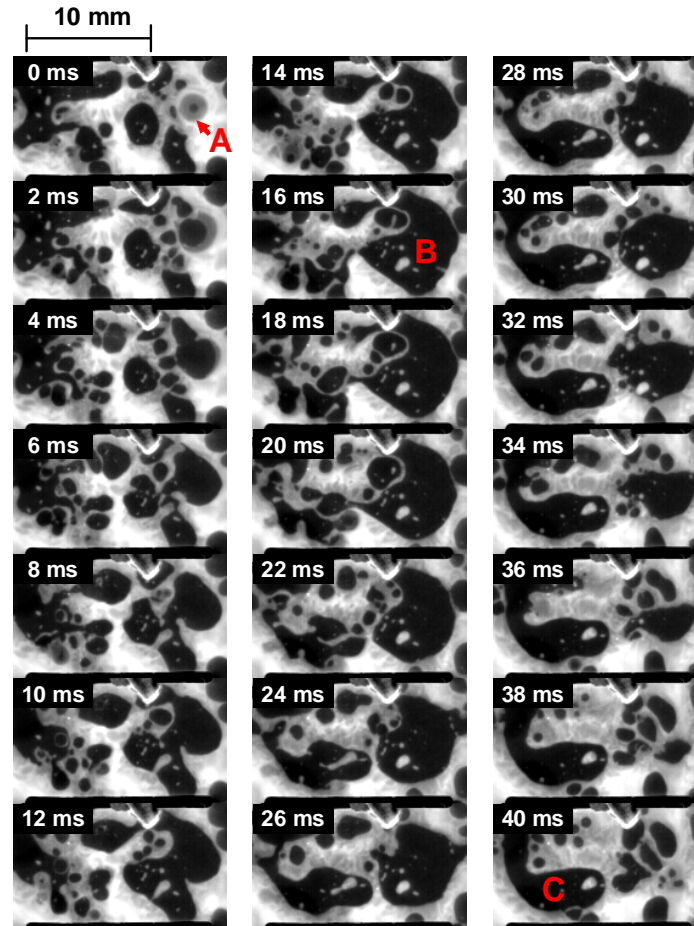

Fig. 10: IR images for liquid (bright) and vapor (dark) phase distribution on the wafer heater surface during nucleate boiling of water at high heat flux (~500 kW/m²). 'A' marks a bubble nucleation event. The dry spot underneath the bubble rapidly grows due to intense evaporation heat transfer near the liquid-vapor-solid contact line and then merges with the nearby dry spots, forming a larger dry patch, marked as 'B' in the 16-ms image. A large mushroom bubble must be hovering above the dry area, though we could not directly verify this, because the HSV images were too chaotic at such high heat flux. The departure of the mushroom bubble causes the dry patch to shrink gradually, and eventually be rewetted by the incoming flow of the surrounding liquid, as seen between 28 ms and 40 ms. The same life cycles of dry spots/patches are observed over the entire heater surface, for example for the area marked as 'C'.
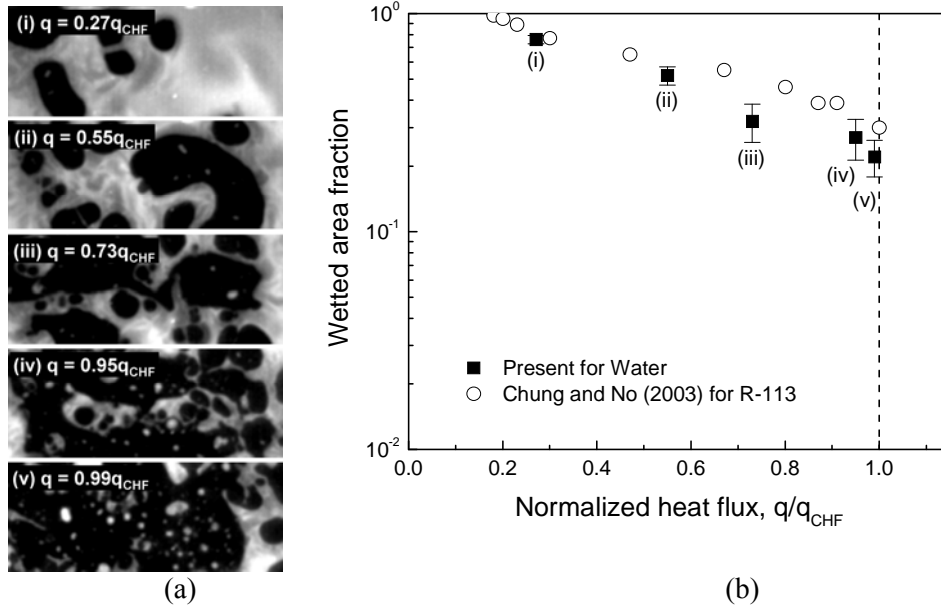
Fig. 11: Phase distribution and wetted area fraction at various heat fluxes (normalized to the CHF): (a) IR images of the heater surface; (b) average wetted area fraction

4. USE OF DATA IN BOILING HEAT TRANSFER MODELING

The type of data presented in the previous sections could prove extremely valuable for validation of ITM-based models of boiling heat transfer, in which the conduction heat transfer problem for the heater is solved for, along with the evaporation phenomena in the fluid. Then, comparing the surface temperature data of, say, Fig. 4 with the surface distribution calculated from the model, the latter can be validated. Similarly, a direct comparison of data and ITM-based predictions for bubble departure and frequency could be completed, as well as for phase distribution (or even wetted area fraction, see Fig. 11b).

Furthermore, traditional semi-empirical models of boiling heat transfer could be informed by the data discussed in Sections 2 and 3. For example, the popular RPI heat flux partitioning model (Kurul and Podowski, 1990), requires knowledge of the key bubble parameters (D_b, NSD, f_b, t_g, t_w), for which generally-valid correlations are not available. In this model the heat removed by the boiling fluid is assumed to be through three contributions, (i) the latent heat of evaporation to form the bubbles (q''_e), (ii) heat expended in re-formation of the thermal boundary layer following bubble departure, or the so-called quenching heat flux (q''_q), and (iii) heat transferred to the liquid phase outside the zone of influence of the bubbles by convection (q''_c). Then the total boiling heat flux is obtained through the addition of the three fluxes as:

$$q''_{tot} = q''_e + q''_q + q''_c \tag{1}$$

Since detailed information for the bubble parameters was obtained from our experiments, it is possible to write expressions for the partitioned heat fluxes that incorporate the contributions of each nucleation site. The latent heat flux can be written as:

$$q''_e = \frac{\pi}{6A} \rho_v h_{fg} \sum_{n=1}^{N_T} \left(f_{b,n} \cdot D_{b,n}^3 \right) \tag{2}$$

where N_T is the total number of nucleation sites. The total quench heat flux is given as:

$$q''_q = \frac{2\pi k_l (T_w - T_{sat})}{A\sqrt{\pi\alpha_l}} \sum_{n=1}^{N_T} \left(D_{b,n}^2 \left(\sqrt{t_{w,n}} f_{b,n} \right) \right) \tag{3}$$

9

The convection heat flux is:

$$q_c^{"} = \left[1 - \frac{\pi}{4A} \sum_{n=1}^{N_T} \left(D_{b,n}\right)^2 \right] h_{turb}\left(T_w - T_{sat}\right) \tag{4}$$

where h_{turb} is the turbulent free-convection heat transfer coefficient from a flat upwards-facing plate, calculated according to the McAdams (1945) correlation. The boiling curve for one test run is shown in Fig. 12 along with the evaporation, quench, convection and total partitioned heat fluxes that have been calculated using the method described above. The model works surprisingly well when considering the amount of independent data that has been fed into it. It is also interesting to note that the quench heat flux is the dominant partitioned heat flux, and not the latent heat flux, as one might expect.
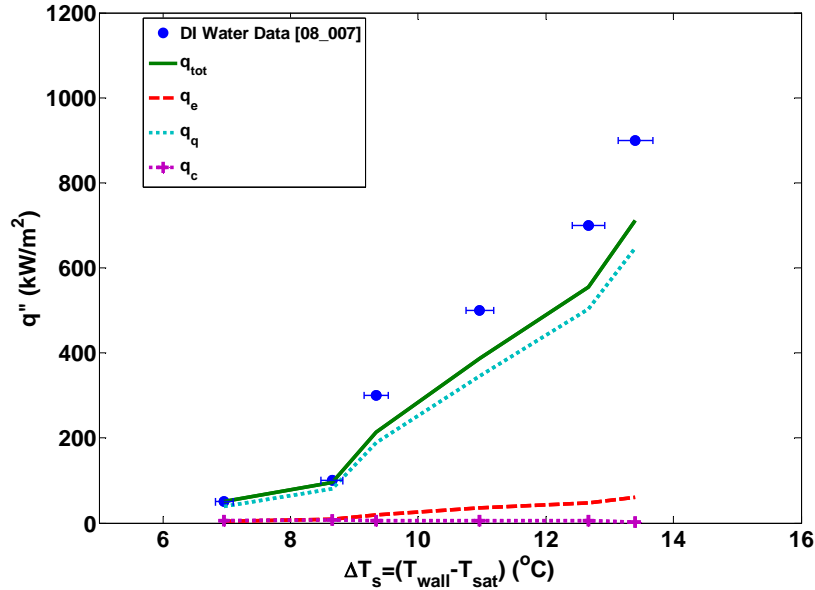

Fig. 12: Comparison of actual boiling curve (●) with RPI partitioning model using corresponding bubble parameters (D_b, NSD, f_b, t_g, t_w) at each superheat for a single DI water test. The uncertainty on the measured values of the heat flux is ~1%.

5. DISCUSSION AND CONCLUSIONS

The value of the technique described in Sections 2 through 4 is to enable direct measurement of boiling heat transfer parameters that have been traditionally difficult to measure. The traditional approaches based on thermocouples and high-speed visualization of the boiling process suffer from several shortcomings; for example, the thermocouples can only measure temperature at discreet locations on the boiling surface, thus no information on the temperature *distribution* about a nucleation site can be obtained. Further, thermocouples (including micro-thermocouples) have relatively long response time, thus are unsuitable for studying the bubble nucleation and growth phenomena, which have time scales of the order of milliseconds. The usefulness of high-speed video is typically limited by poor optical access to the nucleation site and interference from adjacent bubbles. Second-generation two-phase flow diagnostics, such as multi-sensor conductivity and optical probes (Kim et al., 2000; Barrau et al., 1999) and wire-mesh probes (Prasser et al., 1998), can measure bubble diameter and velocity near the boiling surface. However, these approaches are intrusive, and also produce data only at discreet locations within the boiling fluid. On the other hand, X-ray and γ-ray tomography (for measurement of the phase distribution) is non-intrusive, but rather costly/cumbersome as the radiation source has to be rotated at high speed around the test section, which also may limit the time and/or space resolution of the technique. Total reflection (Nishio and Tanaka, 2004) is another non-intrusive approach for measurement of the

phase distribution, though it cannot supply information about the temperature distribution. It was not until the early 2000s that new possibilities for generating time-resolved multi-dimensional data on the bubble nucleation and growth cycle have opened up with the introduction of infrared-based visualization of thermal patterns on the boiling surface by Theofanous et al. (2002). The technique described in this paper, based on synchronized high-speed video and infrared thermometry, builds upon those possibilities. It was shown that data on surface temperature distribution, bubble departure diameter and frequency, growth and wait times, and nucleation site density can be effortlessly measured for all nucleation sites on the heater surface. Moreover, if an IR-transparent heater (e.g silicon wafer) is adopted, the IR camera can directly detect the phase distribution on the boiling surface. All this information could be used for validation of advanced numerical models of boiling heat transfer. Finally, note that, while the data shown in this paper were for saturated pool boiling heat transfer, there is no fundamental difficulty in extending the technique to flow boiling heat transfer (both saturated and subcooled), which is the physical situation of relevance to the nuclear reactor applications.

ACKNOWLEDGEMENTS

REFERENCES

- E. Barrau, N. Rivière, Ch. Poupot and A. Cartellier, "Single and double optical probes in air-water two-phase flows: real time signal processing and sensor performance", *Int. J. Multiphase Flow*, 25(2), 229-256, (1999)
- M.G. Cooper, A.J.P. Lloyd, "The Microlayer in Nucleate Pool Boiling", *Int. J. Heat Mass Transfer*, 12, pp. 895-913, (1969)
- H. J. Chung , H. C. No, (2003), Simultaneous visualization of dry spots and bubbles for pool boiling of R-113 on a horizontal heater, *Int. J. Heat Mass Transfer* 46 2239–2251.
- J. Du, B. Fix, J Glimm, X. Jia, X Li, Y. Li and L. Wu. A simple package for front tracking. *J. Comput. Phys.* 2006 (213) 613-628
- C. Gerardi, "Investigation of the Pool Boiling Heat Transfer Enhancement of Nano-Engineered Fluids by means of High-Speed Infrared Thermography," PhD Thesis, Massachusetts Institute of Technology (2009)
- M. Ishii and T. Hibiki, *Thermo-fluid Dynamics of Two-phase Flow*, Springer, (2006)
- S. Kim, X. Y. Fu, X. Wang and M. Ishii, "Development of the miniaturized four-sensor conductivity probe and the signal processing scheme", *Int. J. Heat Mass Transfer*, 43(22), 4101-4118, (2000).
- L.D. Koffman, M.S. Plesset, (1983), "Experimental observations of the microlayer in vapor bubble growth on a heated solid," *J. Heat Transfer*, 105(3), August, p 625-632, (1983)
- N. Kurul, M.Z. Podowski, "Multidimensional effects in forced convection subcooled boiling", *Proc. 9th International Heat Transfer Conference*, Jerusalem, Israel. pp. 21-25, (1990)
- W.H. McAdams, Heat Transmission (3rd Ed), p. 180, McGraw-Hill, New York (1945)
- S. Nishio and H. Tanaka, (2004), "Visualization of boiling structures in high-heat flux pool-boiling", *Int. J. Heat Mass Transfer*, 47, 4559-4568.
- Osher and R. P. Fedkiw. Level Set Methods: an overview and some recent results. *J. Comput. Phys.* 2001 (169) 463—502
- H.-M. Prasser, A. Bottger, J. Zschau, A new electrode-mesh tomograph for gas–liquid flows, *Flow Measurement and Instrumentation*, 9, 111–119, (1998)

- A. Prosperetti and G. Tryggvason, *Computational methods for multiphase flow*, Ch. 3, Cambridge University Press, (2007).
- W. J. Rider and D. B. Kothe, Reconstructing Volume Tracking, *J. Comput. Phys.* 1998 (141) 112-152
- M. Rudman, A volume-tracking method for incompressible multifluid flows with large density variations, *Int. J. Numer. Meth. Fluids* 1998 (28) 357—378
- R. Scardovelli and S. Zaleski, Direct numerical simulation of free-surface and interfacial flow, *Ann. Rev. Fluid Mech.* 1999 (31) 567—603
- J. A. Sethian. Evolution, Implementation, and Application of Level Set and Fast Marching Methods for Advancing Fronts. *J. Comput. Phys.* 2001 (169) 503—555
- T. G. Theofanous, J. P. Tu, A. T. Dinh and T. N. Dinh, (2002), The Boiling Crisis Phenomenon, J. *Experimental Thermal Fluid Science*, P.I: pp. 775-792, P.II: pp. 793-810, 26 (6-7).
- G. Tryggvason and B. Bunner and A. Esmaeeli and D. Juric and N. Al-Rawahi and W. Tauber and J. Han, S. Nas and Y.-J. Jan. A Front Tracking Method for the Computations of Multiphase Flow. *J. Comput. Phys.* 2001 (169) 708—759
- Y.H. Zhao, T. Masuoka, T. Tsuruta, "Unified Theoretical Prediction of Fully Developed Nucleate Boiling and Critical Heat Flux Based on a Dynamic Microlayer Model", *Int. J. Heat Mass Transfer*, 45, pp. 3189-3197, (2002)